1985MNRAS.214...67S

Mon. Not. R. astr. Soc. (1985) **214,** 67–85

Hotspots in radio galaxies: a comparison with hydrodynamic simulations

Michael D. Smith,* Michael L. Norman, Karl-Heinz A. Winkler and Larry Smarr† *Max-Planck-Institut für Physik und Astrophysik, Institut für Astrophysik, Karl-Schwarzschild-Str. 1, 8046 Garching bei München, FRG*

Accepted 1984 December 13. Received 1984 October 15; in original form 1983 July 21

Summary. Surface brightness distributions are derived for the beam cap of an axisymmetric supersonic jet ramming through its confining medium. The detailed structure and time-evolution of the working surface is computed numerically with a high-resolution gas dynamics code employing a special technique for accurately tracking and preserving the jet boundary. The synchrotron emissivity is assumed to be proportional to the square of the gas pressure inside the jet, and zero outside. The geometry of the beam cap is found to change on a dynamical time-scale, producing an enormous variety of hotspot shapes in a single evolution.

A classification of well-resolved hotspots in radio galaxies is made with which our derived contour maps are compared. Several quite common features of observed hotspots are reproduced, such as:

(i) a bright head with sharp outer edge having a length-to-width ratio 3–5;

(ii) twin wings and single tails extending backwards in the general direction of the nucleus;

(iii) complex subcomponent geometries, including two bright peaks transverse to the source axis.

Hotspots viewed at an angle appear rounder, have smoother edges and have lower dynamic range than when viewed from the side.

Distorted hotspots can be accommodated by a more general model. Three-dimensional simulations should be able to reproduce observed asymmetries. Relativistic beaming effects, non-circular jets, or strong magnetic fields may also contribute to distortion.

1 Introduction

High-resolution numerical simulations of a supersonic jet of gas penetrating into a denser external medium have resolved the pressure, density and flow pattern (Norman *et al.* 1982,

*Permanent address: Department of Astronomy, University of Leicester, Leicester LE1 7RH.
†Permanent address: Departments of Astronomy and Physics, University of Illinois, Urbana, Ill 61801, USA.

© Royal Astronomical Society • Provided by the NASA Astrophysics Data System

Downloaded from https://academic.oup.com/mnras/article-abstract/214/2/67/1031916 by University of California, San Diego user on 15 July 2020

1985MNRAS.214...67S

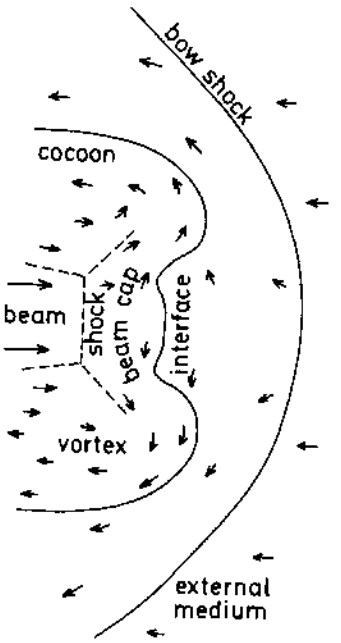


Figure 1. Schematic diagram of the working surface, illustrating the terminology.

hereafter Paper I). Subsequent work (Norman, Winkler & Smarr 1983, hereafter Paper II) has extended our investigation to a wider selection of jet parameters and evolutionary ages. The region of impact at the end of the jet, the 'working surface' or beam cap (*cf.* Fig. 1), maintains a high pressure. For a jet of Mach number M, this pressure is of order M^2 higher than the static pressure of the external medium. Blandford & Rees (1974) proposed that such regions correspond to the highly luminous hotspots observed in radio galaxies. The hotspots are so-called because their relativistic particle pressures, as derived from synchrotron theory arguments, are often much greater than the possible thermal pressure of the surrounding interstellar or intergalactic medium. In this study we shall derive surface brightness distributions from the numerically determined beam caps to compare with the observed hotspots. Our aim is to determine whether a relationship exists between purely hydrodynamic models of the working surface and hotspots in radio galaxies.

The simulations resolve intricate shock, instability and vorticity patterns which are highly non-stationary. Our work produced a different picture from previous attempts by Rayburn (1977) and Wilson & Scheuer (1983, hereafter WS), with the following as crucial factors: (i) the contact discontinuity between the jet material and external medium is kept sharp through the use of the LeBlanc interface tracking technique (Norman 1980; Norman & Winkler 1984), which clearly and unambiguously defines the boundary of the synchrotron-emitting region, whereas this boundary is poorly defined in the works of Rayburn and WS, and (ii) we assume that only the jet material radiates, and not the material between the bow shock and contact discontinuity, as WS assume. The consequences of these two factors, which strongly influence the conclusions of this study, are two-fold: (i) the derived hotspot intensity maps exhibit sharp leading edges when the viewing angle is transverse to the jet axis, and (ii) interfacial instabilities, which earlier works could not properly address, contribute substantially to the non-stationarity of the structure of the working surface and consequent hotspot morphology.

The remainder of this paper is organized as follows. Because of the importance of the underlying hydrodynamic model for the derived hotspot properties, several germane numerical issues are raised and discussed in Section 2 and our own procedure reviewed. In Section 3, our emission model is described and justified, and representative hotspot intensity maps are presented for several stages in the evolution of a jet with high Mach number ($v_{\rm beam}/c_{\rm beam}=6$) and

Downloaded from https://academic.oup.com/mnras/article-abstract/214/2/67/1031916 by University of California, San Diego user on 15 July 2020

© Royal Astronomical Society • Provided by the NASA Astrophysics Data System

1985MNRAS.214...67S

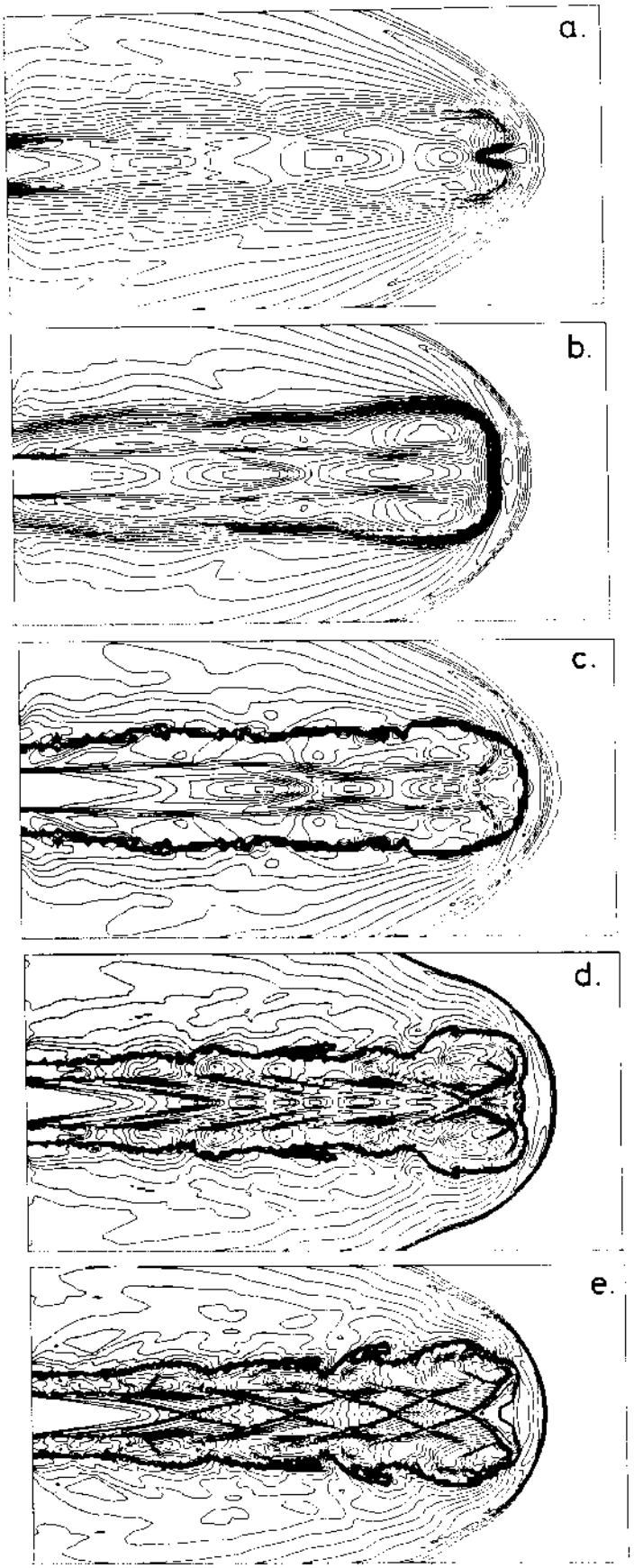


Figure 2. Effects of numerical techniques and resolution on jet structure. (a) Donor cell advection, low resolution ($\Delta R = \Delta Z = R_{\rm beam}/4$); (b) van Leer (1979) monotonic advection, low resolution; (c) same as (b) including LeBlanc interface-tracking; (d) same as (c) but at higher resolution ($\Delta R = \Delta Z = R_{\rm beam}/8$); (e) same as (d) but at highest resolution ($\Delta R = \Delta Z = R_{\rm beam}/16$). Contour lines of gas density are separated by a factor of 1.2. Jet parameters $\eta = 0.1$, $M = 6$; evolutionary time $\tau = 6$. Domain $0 \leqslant R/R_{\rm beam} \leqslant 7.5$, $0 \leqslant Z/R_{\rm beam} \leqslant 30$.

© Royal Astronomical Society • Provided by the NASA Astrophysics Data System

Downloaded from https://academic.oup.com/mnras/article-abstract/214/2/67/1031916 by University of California, San Diego user on 15 July 2020

1985MNRAS.214...67S

low density ($\varrho_{\rm beam}/\varrho_{\rm external}=0.1$). Observed hotspots are classified according to morphology in Section 4, and compared to our predicted maps. The implications of this comparison are discussed in Section 5, as are the possible influences of our assumptions on our results, which are summarized in Section 6. Conclusions and suggestions for future study form the remainder of Section 6.

2 The hydrodynamic model

The problem we consider is the time-dependent penetration of a collimated, supersonic beam of gas into a constant ambient gas. The physical assumptions and the hydrodynamical computations have been described in Papers I and II; the key physical results have been summarized in Smarr, Norman & Winkler (1984, hereafter Paper IV). We shall not repeat their discussion here. Rather, we shall focus on three technical aspects of the computations which have a strong influence on the hydrodynamical model from which the hotspot intensity maps are derived. We consider how (i) the numerical order of accuracy, (ii) zoning resolution, and (iii) the use of a fluid interface to track the jet boundary, affect the structure and dynamics of the end of the jet. These effects are illustrated in Fig. 2, where five numerically different calculations of a Mach 6 ($M\equiv v_{\rm beam}/c_{\rm beam}=6$), low-density ($\eta\equiv\varrho_{\rm beam}/\varrho_{\rm external}=0.1$) jet are compared at equal (dimensionless) evolutionary times $\tau\equiv c_{\rm external}t/R_{\rm beam}=6$. The physical domain displayed is $0\leqslant R/R_{\rm beam}\leqslant 7.5$, $0\leqslant Z/R_{\rm beam}\leqslant 30$.

Fig. 2a, b show the effects of varying the order of accuracy of the numerical advection terms in the Eulerian equations of motion, while holding the grid resolution ($\Delta R=\Delta Z=R_{\rm beam}/4$) constant. These terms dominate the numerical diffusion of sharp features as they propagate through the mesh (see Norman & Winkler 1984). Of particular importance for mapping hotspots is the preservation of the interface between the jet gas and the external medium (*cf.* Fig. 1), which in the context of ideal gas dynamics is a contact discontinuity. Fig. 2a was computed using the first-order accurate donor cell procedure, whereas Fig. 2b was computed using van Leer's (1979) second-order accurate monotonic advection procedure. One can see in Fig. 2a that the position of the fluid interface is completely lost using the highly diffusive donor cell procedure, whereas the interface can be discerned in the higher order accurate computation in Fig. 2b. In addition, other structural elements of the jet interior just barely resolved in Fig. 2b – beam boundary, internal shocks, terminal shocks, cocoon vortices and waves – have been smoothed over in Fig. 2a, leaving an almost featureless rendering of the flow. Notice the spurious indentation of the jet head in Fig. 2a, which is absent in the more accurate computation in Fig. 2b. Notice also that the shape and position of the bow shocks differ, even though the two snapshots were taken at the same time ($\tau=6$). Evidently, an accurate description of the geometry of the jet head influences the overall propagation efficiency (Paper II).

Fig. 2c differs from Fig. 2b only through the application of the LeBlanc fluid interface-tracking procedure (Norman 1980; Norman & Winkler 1984) to the jet boundary. The procedure models the fluid interface as a true contact discontinuity, thereby largely eliminating numerical mass diffusion across the interface. As a result, unstable fluid interfaces are more accurately modelled. One can see in Fig. 2c that the effect of the interface treatment is to bring the jet boundary into sharp focus. Notice that the interior and exterior solutions are substantially the same in Fig. 2b, c as they should be, since the same algorithm was used to compute them.

Although Fig. 2c gives a suggestive rendering of the essential features of the flow, the flow is still under-resolved, with only four zones across the beam radius. For example, it is unclear what is causing the density inhomogeneities within the beam. A clearer picture emerges when the number of zones in each direction is doubled ($\Delta R=\Delta Z=R_{\rm beam}/8$), as is shown in Fig. 2. With eight zones resolving the initial beam radius, we seem to have crossed a threshold where now

Downloaded from https://academic.oup.com/mnras/article-abstract/214/2/67/1031916 by University of California, San Diego user on 15 July 2020

© Royal Astronomical Society • Provided by the NASA Astrophysics Data System

1985MNRAS.214...67S

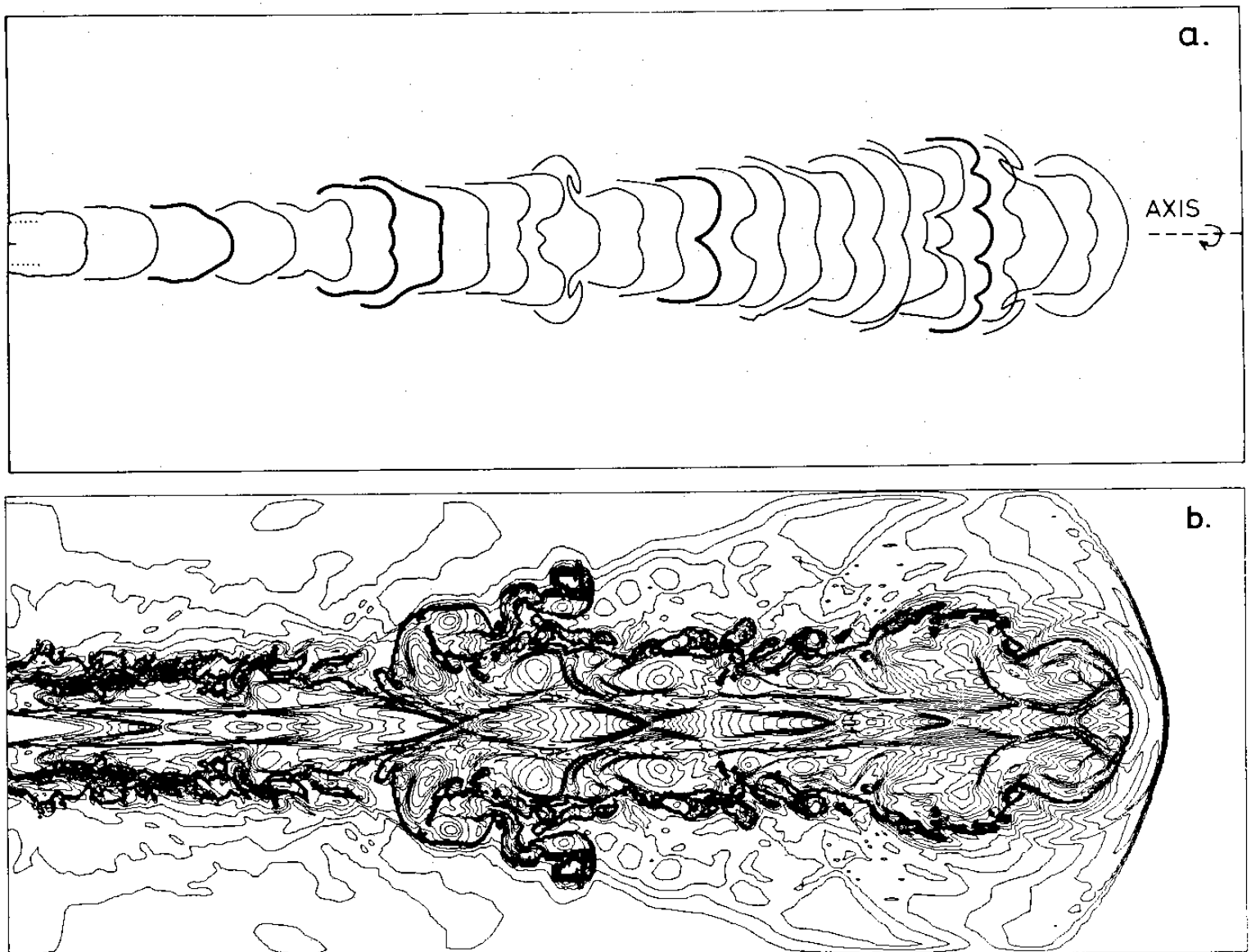


Figure 3. (a) Variations in hotspot brightness and structure are produced by interface oscillations, shown here at equal time intervals $\Delta\tau=1$. Bold lines denote the five cases mapped in Figs 4–8. Dotted lines denote input beam diameter. (b) Density contour plot showing jet structure at $\tau=27$. Jet parameters $\eta=0.1$, $M=6$. Domain $0\leqslant R/R_{\rm beam}\leqslant 15$, $0\leqslant Z/R_{\rm beam}\leqslant 80$.

© Royal Astronomical Society • Provided by the NASA Astrophysics Data System

Downloaded from https://academic.oup.com/mnras/article-abstract/214/2/67/1031916 by University of California, San Diego user on 15 July 2020

1985MNRAS.214...67S

realistic-looking shock structures can appear within the supersonic beam. In addition, we seem to have resolved the largest scale eddies within the cocoon, which takes on a more chaotic appearance than in Fig. 2c. As discussed by Norman, Smarr & Winkler (1984, hereafter paper III), these eddies drive the internal shockwaves within the supersonic beam ('cocoon-dominated' case).

The numerical techniques and resolution used in this study are those of Fig. 2d, with domain $0 \leqslant R/R_{\text{beam}} \leqslant 15$, $0 \leqslant Z/R_{\text{beam}} \leqslant 80$.

In addition to giving a better description of the structure of the hotspot-producing region, the higher resolution computation shows that this region is highly time-dependent. Fig. 3a demonstrates this by showing the shape and position within the full domain of the leading interface at equal time intervals $\Delta\tau = 1$. Generally, the interface oscillates between a globally convex and concave structure as toroidal vortices are shed into the cocoon (*cf.* Fig. 7, Paper I). In the process, the terminal shock cycles alternately between an X-shaped regular reflection structure and a Mach configuration as indicated in Fig. 1. Although the mechanism which drives this oscillation is not completely understood, we find that doubling again the resolution in each dimension as in Fig. 2e leaves the picture unchanged, aside from fine structure. In the next section we show the effect of the oscillation on hotspot structure.

We consider the jet in Fig. 2d a converged solution in the sense that it exhibits all the features and qualitative behaviour of the higher resolution jet in Fig. 2e. Although the detailed boundary shapes at a given time are not identical in both solutions, we find that the leading interface assumes certain generic shapes (*cf.* Fig. 3a) which are similar in both solutions. Since this time-dependence is one of our major findings, and since it is possible that our assumed axisymmetry may amplify the magnitude of the effect, we return to the physical reality of working-surface oscillations in Section 5.

3 Predicted maps

The theoretical maps of radio surface brightness presented below are derived from a jet with initial parameters $M = 6$, $\eta = 0.1$. Fig. 3b shows a density contour plot of the jet at an advanced stage of evolution. As shown in Fig. 3a, the structure of the beam cap constantly changes as low-pressure vortices are built up and released into the cocoon. We have mapped five representative stages chosen for their structural variety. These are indicated by the bold lines Fig. 3a, and correspond to evolutionary times $\tau = 3$, 6, 7, 14, and 23.

The brightness distribution expected from the simulated beam cap is easily calculated with a few simple assumptions. First, we assume that the jet contains thermal plasma, with a $\gamma = 5/3$ equation of state, which governs the dynamics of the flow. Secondly, we ignore the radio emission coming from the beam prior to reaching the working surface shock. Lower surface brightness features such as knots (Paper III) and lobes will be considered in subsequent papers. Relativistic electron and magnetic field energies are then assumed to be strongly amplified by the fluid's passage through the terminal shockwave into the beam cap. We plot surface brightness distributions by producing contour maps of $\int p^n(x)\,dx$ from the thermal pressure p and the depth x through the beam caps. For an appropriate value of n we obtain an estimate to the surface brightness distribution produced by synchrotron radiation.

We shall also assume that the synchrotron radiative lifetime is much longer than the travel time out of the beam cap area. This condition requires a fluid velocity of $0.04c$ in the typical hotspot under minimum energy conditions (Dreher 1981) and less if the magnetic field is below equipartition. We shall not presume equipartition but take the maguetic field to be proportional to the density. The post-shock gas behaves isentropically, resulting in adiabatic losses to the

Downloaded from https://academic.oup.com/mnras/article-abstract/214/2/67/1031916 by University of California, San Diego user on 15 July 2020

© Royal Astronomical Society • Provided by the NASA Astrophysics Data System

1985MNRAS.214...67S

relativistic electrons. It can then be shown that the monochromatic power per unit volume is approximately $L \propto p^2$, for a spectral index close to -0.5.

A final assumption we make is that the jet material *alone* radiates. This assumption is motivated by the high equipartition magnetic field strengths inferred to exist in hotspots ($B_{eq} \approx 10^{-4}$ G; Dreher 1981), whereas the mean intergalactic magnetic field strength has been estimated to be $B_{ig} < 5 \times 10^{-10} \Omega$ G (Ruzmaikin & Sokoloff 1977), where Ω is the mean density of the intergalactic medium normalized by the closure density. Thus, even if particle energy densities were uniform throughout the interaction region, synchrotron emission from outside the jet boundary would be negligible. These simple assumptions, while crucial, enable us to simulate radio maps and will be reconsidered in Sections 4 and 5 in retrospect of the comparison.

The resulting contour maps are shown in Figs 4–8. The distributions of thermal pressure and gas density from which the maps are derived are included for comparison. The pressure plots highlight shockfronts, whereas the density plots display the position of the contact discontinuity separating the low-density jet gas from the shocked external gas. The contours are arranged in equal logarithmic intervals corresponding to factors of 1.2 between levels. The intensity integration has been made for two lines-of-sight making angles of 90° (transverse) and 45° with respect to the axis of jet propagation.

The most striking feature of the emission maps when viewed from 90° is their sharp leading edges, which in general conform to the shape of the bounding contact surface (*cf.* Fig. 4). An exception is shown in Fig. 7. Here, the concave geometry of the source means that the greatest path length of emitting material is off-axis, since we are integrating through a figure of revolution. The result is a hotspot with a sharp leading edge and two bright subcomponents transverse to the source axis. Similarly, the corrugation of the contact surface in Fig. 8 caused by incipient Rayleigh–Taylor instability leads to a hotspot with multiple subcomponents.

A second noteworthy feature of the 90° maps is edge brightening, seen as wings of emission above and below the source axis behind the leading edge of the hotspot. The origin of this feature can be seen most clearly in Fig. 5. Generally, the high-pressure gas in the beam cap escapes into the cocoon through a channel just inside the contact discontinuity but outside the low-pressure 'eye' visible in Fig. 5. Since we have assumed that the synchrotron emissivity scales as p^2, edge-brightening results. Thus, the wings of emission trace the primary escape route of radiating material leaving the working surface.

One final feature of the 90° maps in Figs 5 and 8 worth mentioning is the existence of an emission knot on axis but upstream of the leading emission plateaux. Such knots are produced immediately downstream of the X-shaped shock configurations which we commonly find within supersonic beams (*cf.* Fig. 3b). In Paper III we discuss how these internal shockwaves are driven by the large-scale vortices which are shed from the working surface into the cocoon. The emission knot in Fig. 5 is produced by one such event.

When viewed from 45° to the axis of jet propagation, the hotspots lose their sharp leading edges, although some clustering of contour lines remain. Generally, the hotspots become rounder, with the intensity maximum moving closer toward the centroid of emission. Fig. 7 shows that transverse double hotspots do not produce a torus of emission when viewed obliquely. The emission wings seen at a projection angle of 90° also disappear; the emission ridge in Fig. 8 becomes a broad plateau.

4 Comparison

Before attempting a comparison, we shall first classify observed hotspots by their structural characteristics. A 'category' of hotspots requires several examples. Various quite common

Downloaded from https://academic.oup.com/mnras/article-abstract/214/2/67/1031916 by University of California, San Diego user on 15 July 2020

© Royal Astronomical Society • Provided by the NASA Astrophysics Data System

1985MNRAS.214...67S

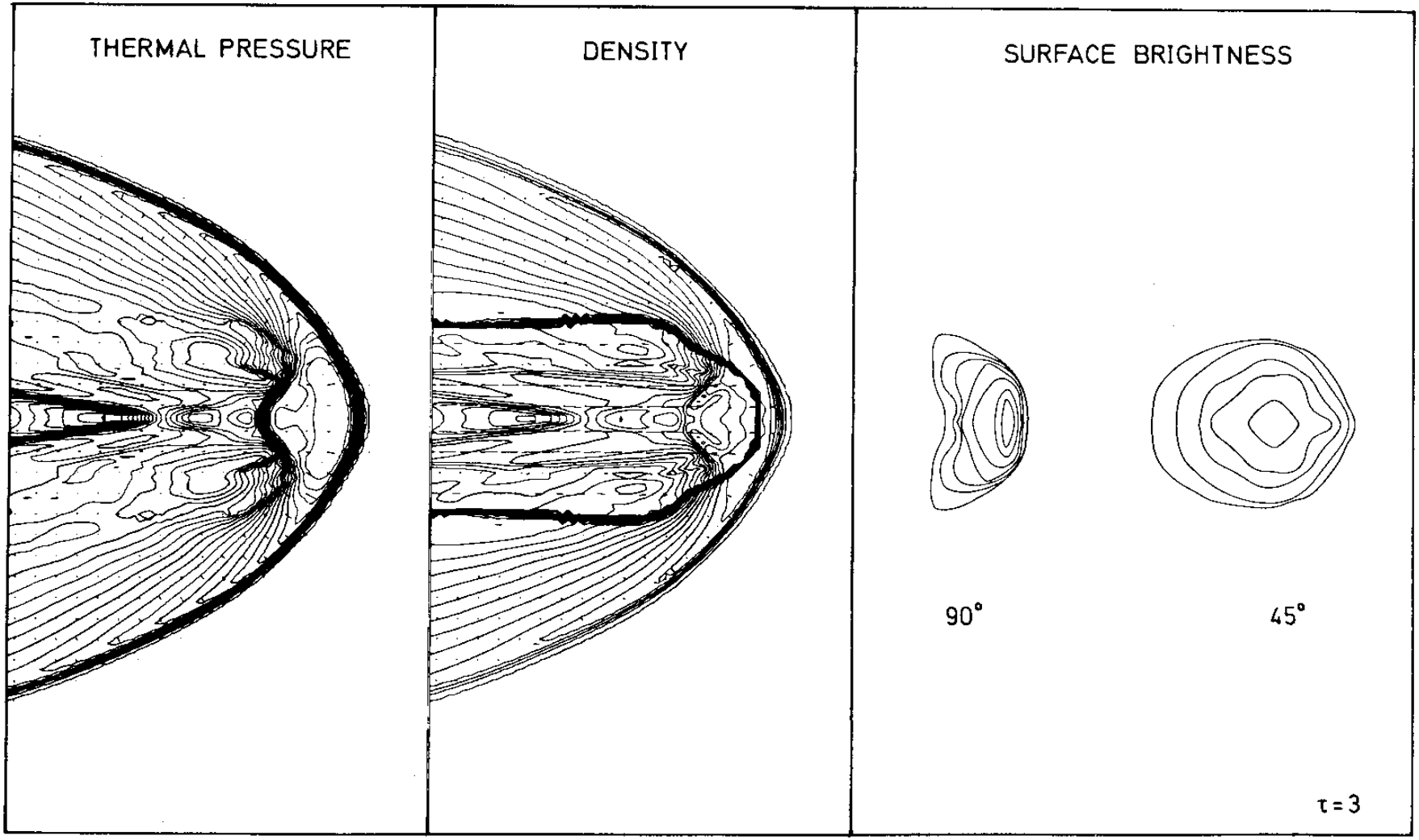


Figure 4. Logarithmic contour plots of pressure, density, and surface brightness for the Mach 6 jet with density ratio 0.1 at time $\tau = 3$. Intensity ranges: $\Delta I(90°) = 160$, $\Delta I(45°) = 35$.

© Royal Astronomical Society • Provided by the NASA Astrophysics Data System

Downloaded from https://academic.oup.com/mnras/article-abstract/214/2/67/1031916 by University of California, San Diego user on 15 July 2020

1985MNRAS.214...67S

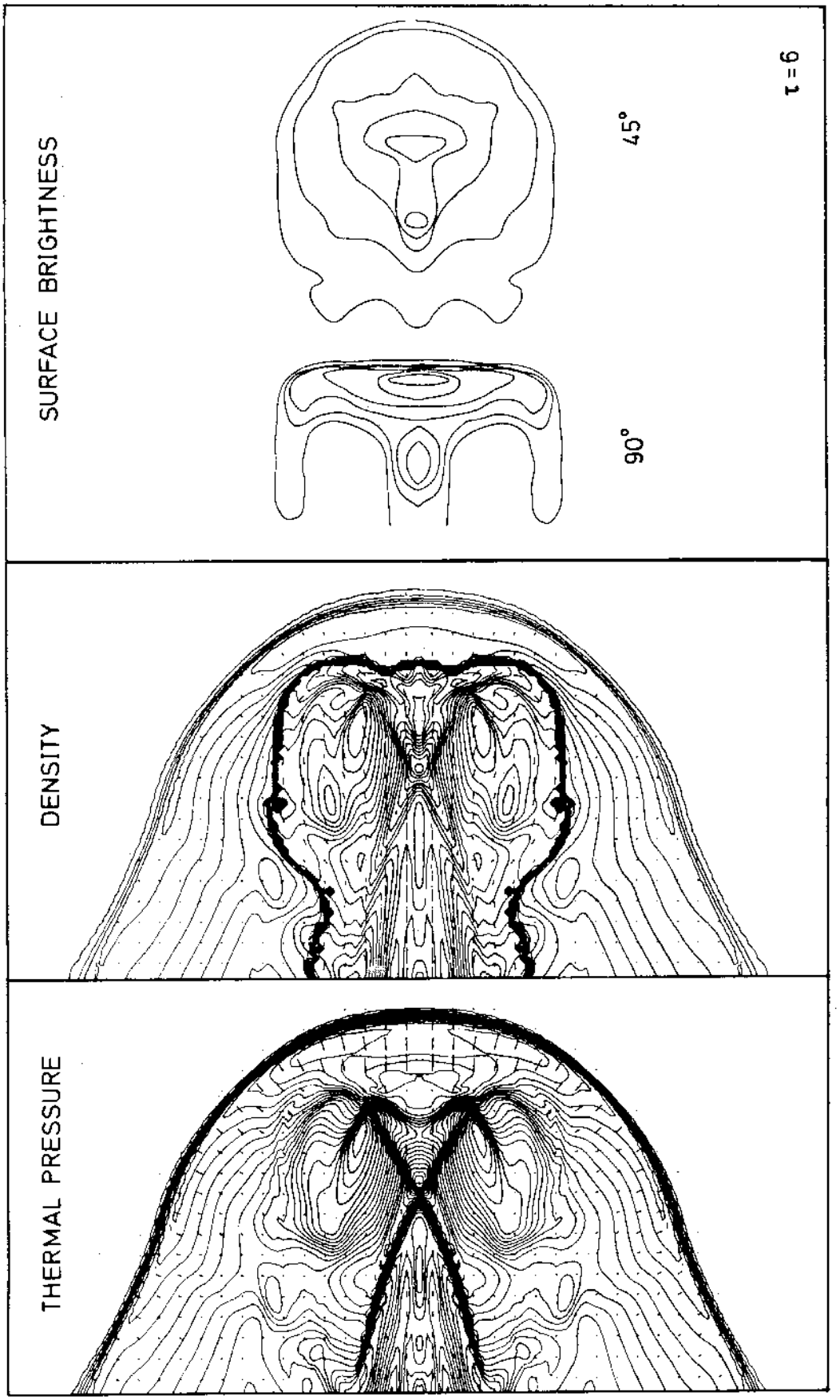


Figure 5. Same as Fig. 4 at $\tau=6$. Intensity ranges: $\Delta I(90°)=100$, $\Delta I(45°)=47$.

© Royal Astronomical Society • Provided by the NASA Astrophysics Data System

Downloaded from https://academic.oup.com/mnras/article-abstract/214/2/67/1031916 by University of California, San Diego user on 15 July 2020

1985MNRAS.214...67S

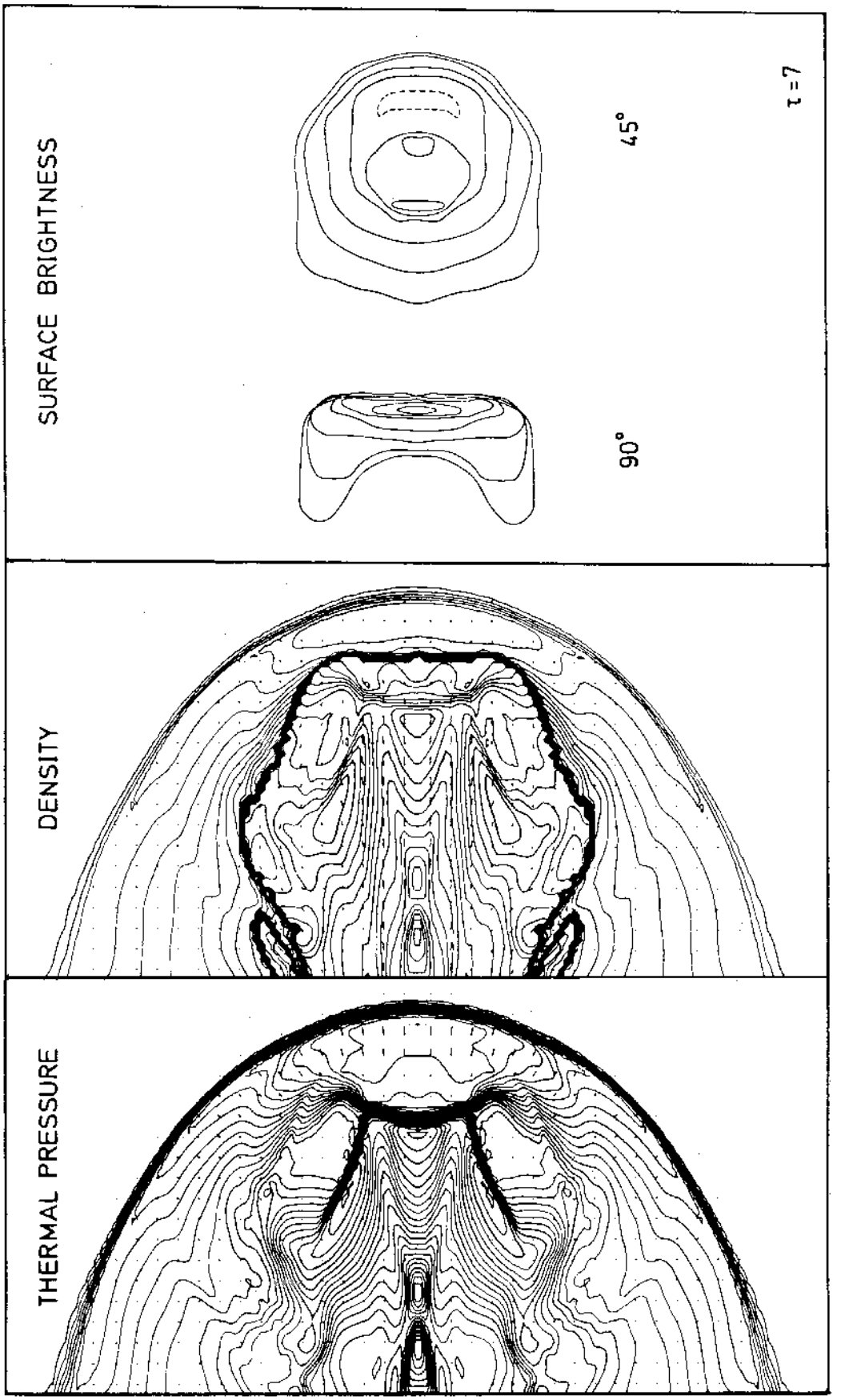


Figure 6. Same as Fig. 4 at $\tau=7$. Intensity ranges: $\Delta I(90^\circ)=90$, $\Delta I(45^\circ)=38$.

Downloaded from https://academic.oup.com/mnras/article-abstract/214/2/67/1031916 by University of California, San Diego user on 15 July 2020

© Royal Astronomical Society • Provided by the NASA Astrophysics Data System

1985MNRAS.214...67S

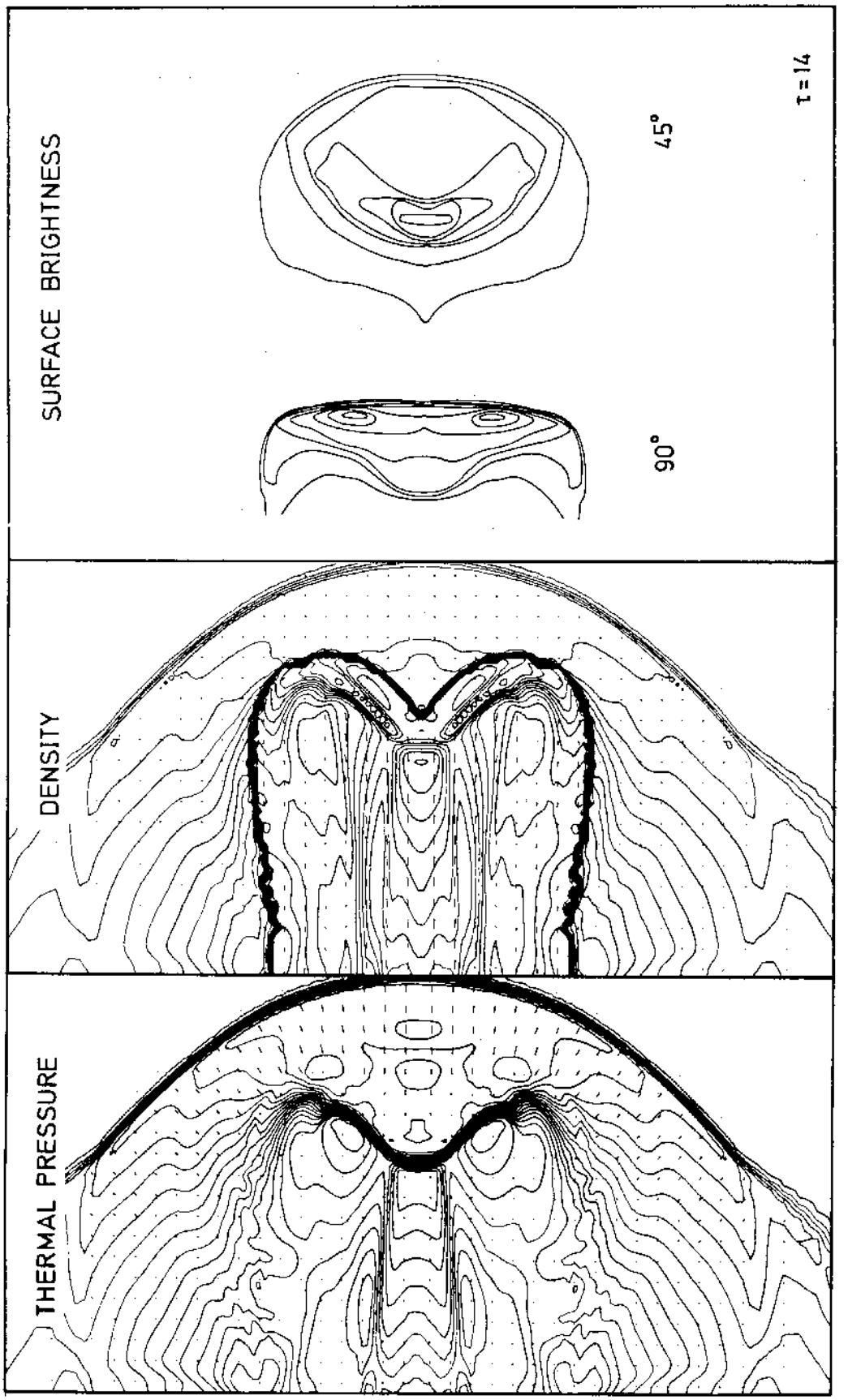


Figure 7. Same as Fig. 4 at $\tau=14$. Intensity ranges: $\Delta I(90°)=150$, $\Delta I(45°)=45$.

© Royal Astronomical Society • Provided by the NASA Astrophysics Data System

Downloaded from https://academic.oup.com/mnras/article-abstract/214/2/67/1031916 by University of California, San Diego user on 15 July 2020

1985MNRAS.214...67S

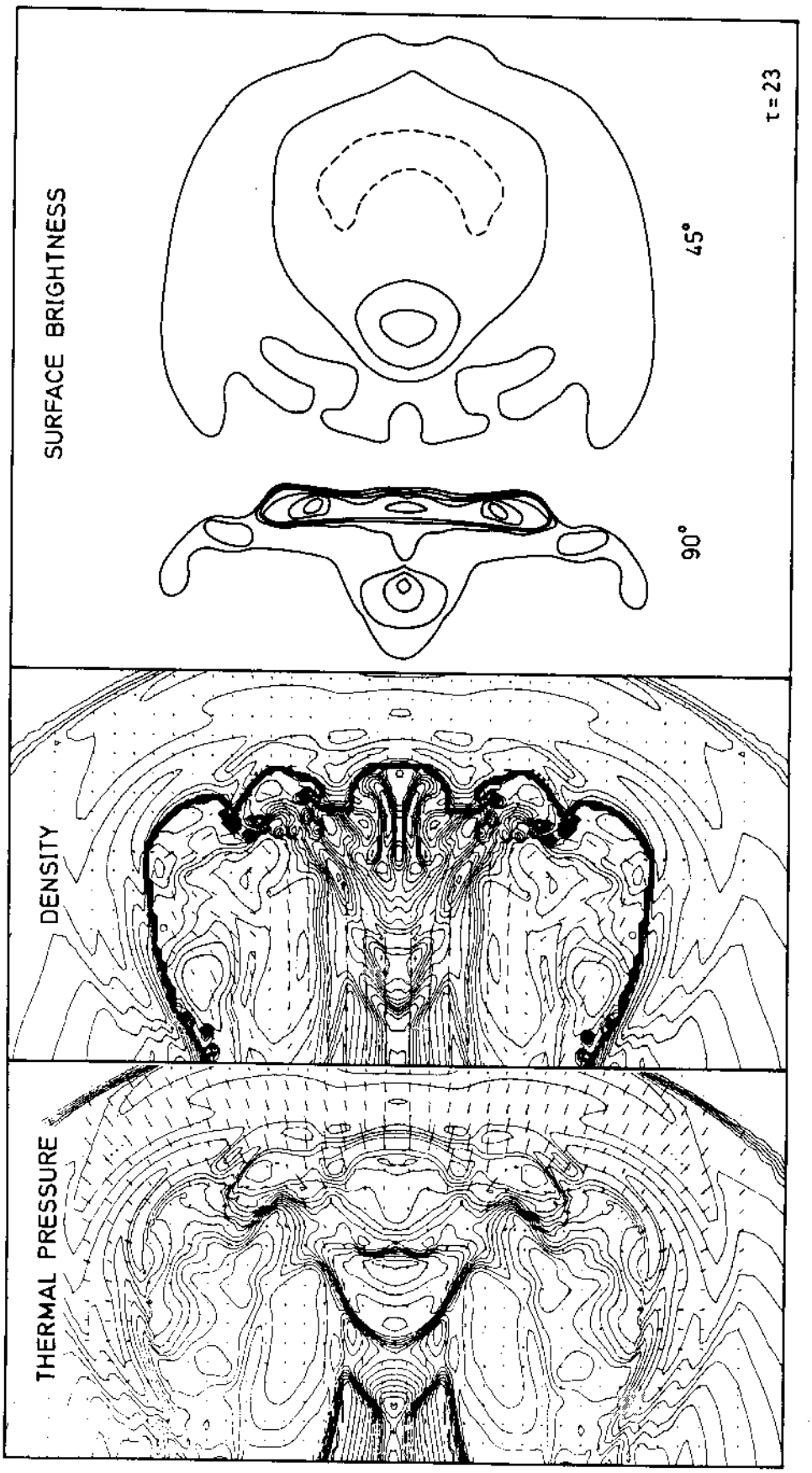


Figure 8. Same as Fig. 4 at $\tau = 23$. Intensity ranges: $\Delta I(90°) = 12$, $\Delta I(45°) = 15$.

Downloaded from https://academic.oup.com/mnras/article-abstract/214/2/67/1031916 by University of California, San Diego user on 15 July 2020

© Royal Astronomical Society • Provided by the NASA Astrophysics Data System

1985MNRAS.214...67S

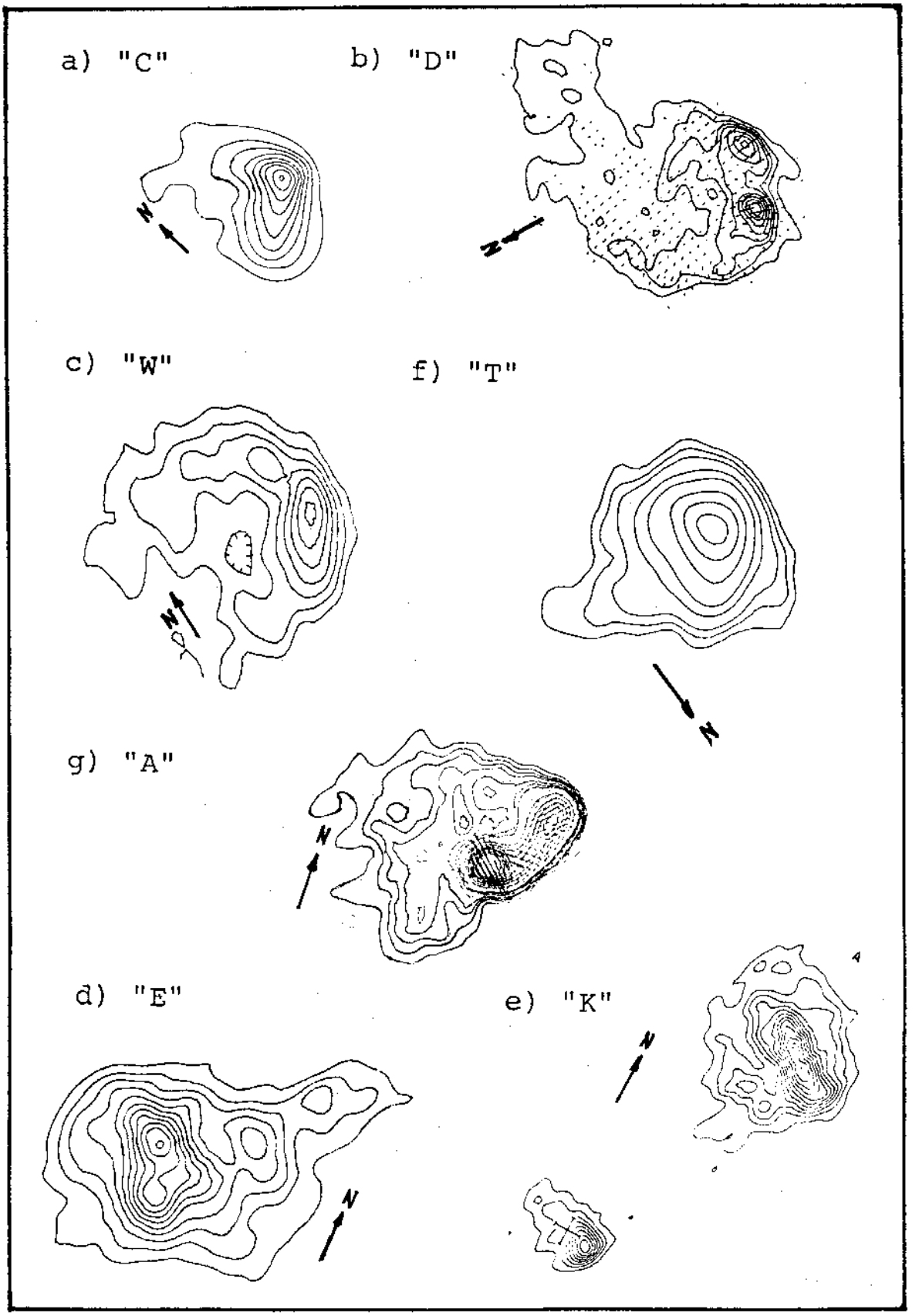


Figure 9. Sample hotspots illustrating our classification scheme described in Section 4. (a) 3C219S from Perley *et al.* (1980), with permission from the *Astronomical Journal*; (b) 3C390.3S, (c) 3C234W, (d) Cyg A Se, (e) Cyg A NW from Dreher (1981), with permission from the *Astronomical Journal*; (f) 3C382E from Dreher, in preparation; (g) 3C20W from Laing (1982), with permission from D. Reidel Publishing Company.

Downloaded from https://academic.oup.com/mnras/article-abstract/214/2/67/1031916 by University of California, San Diego user on 15 July 2020

© Royal Astronomical Society • Provided by the NASA Astrophysics Data System

1985MNRAS.214...67S

characteristics have been found. Here we shall classify hotspots according to the following properties:

Type C: A compact hotspot with a single peak;
Type D: Two bright peaks within the main component;
Type T: A single trail of emission stretching back towards the nucleus;
Type W: Two wings of emission extending back from a main ridge;
Type E: A region of diffuse emission ahead of the region of peak brightness;
Type A: Wings or a ridge, asymmetric about the overall source axis;
Type K: A knot of emission situated behind the hotspot but not on the overall source axis.

The categories are not mutually exclusive, so a hotspot may belong to more than one category. Table 1 presents examples of well-resolved hotspots classified according to this scheme. Fig. 9 shows radio surface-brightness maps of observed hotspots which we believe typify their classes.

Although our classification scheme is observationally motivated, it possesses a certain logical basis as well. Thus, classes C and D refer to the number of subcomponents; a class M for multiple

Table 1. Observed and simulated examples of characteristic hotspots.

Type	Examples		Figure*
C	3C 234E (D)	3C 219S (P)	3C 244.1N (L)	4a, b; 6a, b
D	3C 379.1N (L)	3C 61.1S (D)	3C 390.3S (D)	7a
T	3C 35N (B)	3C 382N (Da)	3C 244.1S (L)	5a, b; 8a
W	3C 389.3s (D, L)	3C 234W (D)	3C 20E (La)	5a, 6a, 7a
E	3C 35S (B)	CygA E (D)	CygA W (D)	7b, 8b
A	3C 33S (D)	3C 205S (L)	3C 20W (La)	–
K	CygA W (D)	3C 390.3N (D, L)	3C 351N (L)	–

*a=90°, b=45°.
(B)=van Beugel (1980).
(D)=Dreher (1981).
(Da)=Dreher (private communication).
(L)=Laing (1981).
(La)=Laing (1982).
(P)Perley *et al.* (1980).

subcomponents has not been included because of the lack of good examples. Classes T, W, and E refer to various extensions of emission from the main component(s), and classes A and K deal with hotspots which are asymmetric about the overall source axis. Our classification scheme does not include a special class for hotspots with very steep outer edges, because this is such a common property of well-resolved hotspots (Dreher 1981).

We can immediately see from Table 1 and Figs 4–8 that the first five properties are successfully reproduced by the simulations. Indeed, the computed hotspots typically exhibit more than one characteristic, as do observed hotspots. The asymmetric hotspots (Type A) obviously cannot be simulated by axisymmetric calculations. However, type A hotspots often exhibit the morphological attributes of the axisymmetric classes (e.g. the wings in 3C 33S, Dreher 1981), and thus appear not to be fundamentally different from the computed hotspots. Although axisymmetric, type D hotspots do not become ring-shaped when not in the plane of the sky. Except when observed edge-on, the torus of emission tends to be washed under by the surrounding diffuse emission.

Although non-axisymmetric, the type K morphology, which has been discussed by Laing (1982) and Kronberg & Jones (1982, hereafter KJ), is not at variance with our model if one interprets the knot (active subcomponent in Laing's terminology, and 'B' hotspot in KJ's

Downloaded from https://academic.oup.com/mnras/article-abstract/214/2/67/1031916 by University of California, San Diego user on 15 July 2020

© Royal Astronomical Society • Provided by the NASA Astrophysics Data System

1985MNRAS.214...67S

classification) as a point of jet deflection, and the outermost hotspot (diffuse subcomponent in Laing's terminology, and 'A' hotspot in KJ's classification) as the jet terminus. This interpretation is made plausible by noticing that (i) in the case of 3C 20E the sharp edge of the diffuse subcomponent is on the opposite side of the active subcomponent (Laing 1982), (ii) in the case of Cyg AW, the jet points to knot B (Perley, Cowan & Dreher, in preparation). The main ridge in knot A is nearly transverse to the knot A–knot B axis (Dreher 1981), and the observed magnetic field orientation (Hargrave & Ryle 1974) is longitudinal in knot B but transverse in knot A, (iii) the morphologies of the 'A' hotspots are similar to our predicted maps (e.g. 3C 20E, Laing 1982), with the axis of symmetry corresponding to the 'A' hotspot–'B' hotspot axis.

Smith (1984) has shown how small-angle jet deflections near the working surface can be amplified quickly to produce large-angle ($\lesssim 180°$) deflections. A 'B' hotspot would be interpreted as the location of a strong oblique shock effecting a sudden bend in the supersonic beam. Observations of the detailed morphology of the deflecting knots should show a preferential bunching of contour lines to the outside of the bend if this picture is correct. This is indeed observed in 3C 390.3N and Cyg AW (Dreher 1981).

The morphology of hotspots will probably become more complex when observed at higher resolution. We expect new VLA maps to increase the number of categories and, as with types of radio galaxies, to increase the number of unclassifiable hotspots.

5 Implications

The overriding purpose of this study is to determine whether a relationship exists between purely hydrodynamic models of the working surface of a supersonic jet and hotspots in radio galaxies as first proposed by Blandford & Rees (1974). A detailed comparison of observed and theoretical intensity maps constitutes a test of the validity of the fluid description of the bulk properties of extended extragalactic radio sources and jets (see Begelman, Blandford & Rees 1984 for a review). In view of the good agreement between the observed and predicted hotspots described in Section 4, we conclude that a fluid description is at least *consistent* with the observations. The stronger conclusion that fluid dynamics is a *good* model of the bulk physics of hotspots is motivated by the reproduction of specific observed morphological features which have heretofore lacked a clear physical interpretation. The three most striking features which our model accounts for are: (i) the steep decline of intensity observed at the leading edges of many well-resolved hotspots (*cf.* Fig. 9a), (ii) the 'double–double' morphology: two bright subcomponents transverse to the source axis (*cf.* Fig. 9b), and (iii) emission wings extending back towards the source (*cf.* Fig. 9c). The physical interpretations of these features have been given in Section 3.

Having thus gained some confidence in the predictive power of our model, let us turn the argument round and consider the broader implications of the hotspot structures observed.

We have seen that our twin assumptions that there is a sharp interface between the jet and the ambient medium, and that only the jet material radiates detectably, lead to simulated hotspots with a sharp decline of intensity at their leading edges when viewed transversely from the source axis ($\theta=90°$). Dreher (1981) has examined a sample of hotspots with high surface brightness, and finds a typical length-to-width ratio of 4 for the outer edges. The ratio for our simulated hotspots is 3–5, which correlated well in so far as a sample with high surface brightness favours edge-on hotspots (Dreher 1981). This is simply an effect of greater path lengths in edge-on hotspots which yield higher intensities than when viewed obliquely (compare $\Delta I(\theta=90°)$ with $\Delta I(\theta=45°)$ in Figs 4–8). We therefore concur with Dreher's conclusion that a high flatness ratio hotspot with a sharp outer edge is seen nearly edge-on. Thus, the structure of a hotspot is a constraint on the orientation of the source axis with respect to the plane of the sky of a classical double (Class II)

Downloaded from https://academic.oup.com/mnras/article-abstract/214/2/67/1031916 by University of California, San Diego user on 15 July 2020

© Royal Astronomical Society • Provided by the NASA Astrophysics Data System

1985MNRAS.214...67S

radio source, on the determination of source size, and on the question of intrinsic source asymmetry versus relativistic beaming.

Dreher (1981) noted that the sharp edges of hotspots were smooth, which he interpreted as an absence of Rayleigh–Taylor instabilities on the leading contact surface. Dreher concluded that the mass density in such hotspots must be less than or equal to the external density. Our calculations show that low-density jets are also subject to Rayleigh–Taylor instabilities at the working surface (*cf.* Fig. 8). This is because both signs of acceleration are felt at the fluid interface as the working surface oscillates (*cf.* Fig. 3). Fig. 8 shows that the observable consequence of the small-scale instabilities that result are multiple bright subcomponents within a hotspot having a smooth, sharp outer edge (θ=90°).

The existence of sharp leading edges in hotspots implies moreover that the boundary between the jet material and the ambient medium is itself at least as sharp, and thus sensibly modelled as a contact discontinuity. As pointed out above, there will be some mixing across this boundary due to short-wavelength Rayleigh–Taylor instabilities, which will effectively broaden the boundary. This process has been analysed by Allen & Hughes (1983), and studied by Sturtevant and coworkers at the Graduate Aeronautics Laboratory of the California Institute of Technology (private communication). If we adopt the hypothesis that subcomponents are the result of interfacial instabilities, then their size would set an upper limit on the interface thickness since instability at shorter wavelengths would effectively be damped.

It is a general result that longer wavelengths of the Rayleigh–Taylor instability dominate in the non-linear regime (see e.g. Sharp 1984). The concave nose geometry which produces the type-D hotspot shown in Fig. 7 can be interpreted as the longest wavelength axisymmetric mode available to the system. It is likely that the assumption of axisymmetry magnifies the importance and occurrence of this mode, but the fact that observed hotspots show type-D morphologies encourages us to believe that such distortions of the working surface do occur in nature. Laboratory studies and 3-dimensional numerical simulations should shed some light on this issue.

The emission wings denote the path of high-pressure matter backflowing from the beam cap into the cocoon. The length of the predicted emission wings depends crucially on the luminosity–pressure relationship. A lower value of n would enhance the wings relative to the hotspot. Reacceleration within the beam cap and wings, through the second-order Fermi process, would have this effect. The observed wing lengths are, however, in good agreement with the numerical calculations. This comparison was made with maps of similar dynamic range [for instance, the higher resolution maps of 3C 234W only reveal the bright ridge (Dreher 1981)]. We cannot rule out other models; a combination of factors, such as a lower n and some reacceleration, would produce similar wings.

A poloidal magnetic field will have field lines parallel to the velocity vectors. With small velocity changes and a magnetic field frozen-in to the fluid, we have taken the field to be proportional to the density ϱ. A toroidal field frozen-in to the fluid can be perceived as a series of smoke-rings rising from the shock and expanding before encircling the jet as they flow into the cocoon. The field strength is, approximately, proportional to $\varrho^{1/2}$, giving a value of $n\sim1.5$. This will produce longer and brighter wings relative to the ridge. The simplest way to differentiate between the two magnetic field structures is, of course, through polarization maps. The magnetic field generally runs parallel to the rim of the hotspot and along the contours in the tails and bridges (Laing 1981). Thus the poloidal model is more plausible, although the field may be sheared in the cocoon.

Further structure behind the beam cap may result from the vortices (see Fig. 1). Such structure is not displayed in the brightness maps because the vortices have low pressure and are shed into the trailing regions which we have not mapped. Turbulent reacceleration, field shearing and the entrapment of relativistic particles may cause the vortices to brighten above the level of the

Downloaded from https://academic.oup.com/mnras/article-abstract/214/2/67/1031916 by University of California, San Diego user on 15 July 2020

© Royal Astronomical Society • Provided by the NASA Astrophysics Data System

1985MNRAS.214...67S

surrounding cocoon. The vortices are caused by large-scale fluid instabilities in the beam cap (Paper I), and hence may be resolvable. We believe that these vortices are related to the closed loops of magnetic field observed in the lobes of 3C 20W (Laing 1982) and 3C 390.3N (Laing 1981).

There is no *a priori* reason for hotspots to be axisymmetric. The type-K knots may be the regions of deflection of a jet, which, as a result, is not in direct impact with the external medium. Distorted hotspots then result (Smith 1984).

If the beam cap itself moves relativistically, the time delay between the near and far sides of an individual beam cap would cause it to appear rotated (Eichler & Smith 1983). A statistical upper limit of $0.2c$ has been derived for radio galaxies from consideration of relative distances from the nucleus of the two hotspots in a double source (Longair & Riley 1979). The effect is to make the hotspot on one side of the nucleus (approaching) appear more edge-on. The opposite effect occurs for the receding hotspot. One should also anticipate distortion of the structure of beam caps by relativistic effects. A similar intrinsic beam cap and cocoon are expected in a relativistic fluid version (Blandford & Rees 1974), although a portion of the flow in a beam cap is deflected towards the observer and its emission is enhanced by relativistic beaming. This is another means by which symmetry can be broken and fine structure can appear. Wilson & Scheuer (1983) have considered the effect of relativistically moving hotspots. We remark here that the two hotspots of a classical radio galaxy may have vastly different intrinsic sizes and luminosities because of the oscillations in beam cap structure. Furthermore, the cocoon gas can be flowing back towards the nucleus, brightening the receding hotspot.

6 Conclusions

We have shown that an axisymmetric supersonic gas jet ramming into a constant external medium produces a hotspot with a spatially and temporally varying surface brightness. A strong non-uniform shock acts to thermalize the bulk kinetic energy of the jet as it enters the beam cap (*cf.* Fig. 1). The model assumes that this shock produces a spectrum of comoving relativistic electrons which radiate at radio frequencies in the shocked jet gas.

We find in general that a hotspot's brightness, flatness, and sharpness of its leading edge depend strongly upon viewing angle. Seen edge-on, a hotspot appears brighter and flatter because of the longer line-of-sight through the beam cap, which is typically pancake-shaped. Projection effects will make the hotspot appear rounder, have smoother edges, and have lower dynamic range.

The model agrees with observed hotspots, reproducing several quite common characteristics such as:

(i) a compressed head with a sharp outer edge and a length several times longer than the width;
(ii) twin wings and single tails extending backwards in the general direction of the nucleus;
(iii) subcomponents which are comparable to the mini-doubles in individual hotspots.

On the basis of this detailed agreement, we conclude that a fluid description of the bulk properties of plasma jets is not only consistent with observations, but is a good model with some predictive power. One is encouraged, therefore, to continue modelling radio jets within the framework of hydrodynamics and magnetohydrodynamics, and to map the entire flow field for comparison with detailed observations of jets, knots, lobes, and cocoons. Work is now in progress to map the parameter survey of jets described in Paper II, to investigate the influence of Mach number, density ratio, viewing angle, and emission model on surface brightness distribution.

Small-scale Rayleigh–Taylor instabilities within the head produce multiple subcomponents in the hotspot, and contribute to its time-varying nature. Variations in hotspot structure occur on a time-scale given by (beam radius)/(external sound speed). For a beam radius of 300 pc and a sound speed of 3×10^8 cm s^{-1}, the resultant time-scale is 10^5 yr – undetectably slow. For further

Downloaded from https://academic.oup.com/mnras/article-abstract/214/2/67/1031916 by University of California, San Diego user on 15 July 2020

© Royal Astronomical Society • Provided by the NASA Astrophysics Data System

1985MNRAS.214...67S

evidence of working surface variations we therefore need observations of yet higher resolution or a statistical comparison with a large sample.

We have discussed various possibilities for improving the agreement. Asymmetries in the fine structure are commonly observed, implying a significant alteration to the symmetric model. The final shock need not to be perpendicular to the source axis, thus deflecting a large fraction of fluid to one side. A flattened jet would lead to cigar-shaped beam caps and can also account for elongated hotspots. Relativistic flow, as seems inevitable in Cygnus A (Dreher 1981), can lead to distorted hotspots.

Future numerical studies should investigate the dynamics of 3-dimensional beam caps, and address the additional observables of polarization, field orientation, and spectral index distribution. This will necessitate the construction of far more complicated physical models than we have described here, and will generally require 3-dimensional simulations. In view of the influence of numerical techniques and resolution on the accuracy of the underlying flow description (Section 2), and the limited resolution currently attainable in 3-dimensions on machines such as the CRAY 1, one should first seek comprehensive solutions to more limited problems rather than vice versa.

Acknowledgments

We are extemely grateful to Dr Dreher for use of his unpublished hotspot observations, and to the referee for useful comments. MS and MN thank the Max-Planck-Institut für Astrophysik and the Astronomy Department, University of Leicester, respectively, for their hospitality while this work was being finalized. LS acknowledges partial financial support under NSF grants nos. PHY 80-01496 and 83-08826.

References

Allen, A. J. & Hughes, P. A., 1983. *Mon. Not. R. astr. Soc.*, **202,** 935.
Begelman, M. C., Blandford, R. D. & Rees, M. J., 1984. *Rev. Mod. Phys.*, **56,** 255.
Blandford, R. D. & Rees, M. J., 1974. *Mon. Not. R. astr. Soc.*, **169,** 395.
Dreher, J. W., 1981. *Astr. J.*, **86,** 833.
Eichler, D. & Smith, M. D., 1983. *Nature*, **303,** 779.
Hargrave, P. J. & Ryle, M., 1974. *Mon. Not. R. astr. Soc.*, **166,** 305.
Kronberg, P. P. & Jones, Y. W., 1982. In: *Extragalactic Radio Sources, IAU Symp. No. 97*, p. 157, eds Heeschen, D. & Wade, C., Reidel, Dordrecht, Holland (KJ).
Laing, R. A., 1981. *Mon. Not. R. astr. Soc.*, **195,** 261.
Laing, R. A., 1982. In: *Extragalactic Radio Sources, IAU Symp. No. 97*, p. 161, eds Heeschen, D. & Wade, C., Reidel, Dordrecht, Holland.
Longair, M. S. & Riley, J. M., 1979. *Mon. Not. R. astr. Soc.*, **188,** 625.
Norman, M. L., 1980. *PhD thesis*, University of California. Davis Lawrence Livermore Laboratory, Report UCRL-52946.
Norman, M. L., Smarr, L., Winkler, K.-H. A. & Smith, M. D., 1982. *Astr. Astrophys.*, **113,** 285 (Paper I).
Norman, M. L., Winkler, K.-H. A. & Smarr, L., 1983. In: *Astrophysical Jets: Proceedings of an International Workshop held in Torino, Italy*, p. 227, eds Ferrari, A. & Pacholczyk, A. G., Reidel, Dordrecht, Holland (Paper II).
Norman, M. L., Smarr, L. & Winkler, K.-H. A., 1984. In: *Numerical Astrophysics: A Festschrift in Honor of James R. Wilson*, eds Centrella, J., LeBlanc, J., LeBlanc, M. & Bowers, R., Jones and Bartlett, Boston (Paper III).
Norman, M. L. & Winkler, K.-H. A., 1984. *Astrophysical Radiation Hydrodynamics*, eds Winkler, K.-H. A. & Norman, M. L., Reidel, Dordrecht, Holland.
Perley, R. A., Bridle, A. H., Willis, A. G. & Fomalont, E. B., 1980. *Astr. J.*, **85,** 499.
Rayburn, D. R., 1977. *Mon. Not. R. astr. Soc.*, **179,** 603.
Ruzmaikin, A. A. & Sokoloff, D. D., 1977. *Astr. Astrophys.*, **58,** 247.
Sharp, D. H., 1984. In: *Fronts, Interfaces, and Patterns*, ed. Campbell, J., *Physica*, in press.

Downloaded from https://academic.oup.com/mnras/article-abstract/214/2/67/1031916 by University of California, San Diego user on 15 July 2020

© Royal Astronomical Society • Provided by the NASA Astrophysics Data System

1985MNRAS.214...67S

Smarr, L., Norman, M. L. & Winkler, K.-H. A., 1984. In: *Fronts, Interfaces, and Patterns*, ed. Campbell, J., *Physica*, in press (Paper IV).
Smith, M. D., 1984. *Mon. Not. R. astr. Soc.*, **211,** 767.
van Breugel, W., 1980. *PhD thesis*, Leiden.
van Leer, B., 1979. *J. Comp. Phys.*, **32,** 101.
Wilson, M. J. & Scheuer, P. A. G., 1983. *Mon. Not. R. astr. Soc.*, **205,** 449 (WS).

Downloaded from https://academic.oup.com/mnras/article-abstract/214/2/67/1031916 by University of California, San Diego user on 15 July 2020

© Royal Astronomical Society • Provided by the NASA Astrophysics Data System